Review Article Adv. Mat. Lett. 2013, **4**(7), 508-521 ADVANCED MATERIALS Letters

www.amlett.com, www.amlett.org, DOI: 10.5185/amlett.2012.12493 Published online by the VBRI press in 2013

Recent advancements on warfare agents/metal oxides surface chemistry and their simulation study

Neha Sharma and Rita Kakkar*

Department of Chemistry, University of Delhi, Delhi 110 007, India

*Corresponding author. Tel: (+91) 1127666313; E-mail: rkakkar@chemistry.du.ac.in

Received: 31 December 2012, Revised: 10 January 2013 and Accepted: 12 January 2013

ABSTRACT

Chemical warfare agents (CWA) have been used in the World Wars and in terrorist attacks, and hence there is an urgent need to find means of their decontamination. Metal oxides offer a rapid means of their disposal, since they contain reactive Lewis acid and basic sites, on which adsorption of the CWA, and subsequent hydrolysis, can take place. Destructive adsorption of CWA on metal oxides yields non-toxic products. Nanoscale metal oxides display enhanced reactive properties toward warfare agents due to their high surface area, large number of highly reactive edges, corner defect sites, unusual lattice planes and high surface to volume ratio. Both experimental and theoretical studies have established that decomposition of nerve agents is facilitated on nanoscale Al_2O_3, MgO, CaO, TiO_2, ZnO and small edge and corner clay mineral fragments. Compared to sulfur mustard, nerve agents are more potent. We first briefly describe their mode of action. Many experimental and theoretical studies have been performed to study their decomposition on various metal oxide surfaces, such as MgO, CaO, Al_2O_3, TiO_2, V_2O_5, and clay minerals. The results of these studies are reviewed here. Photochemical degradation on TiO_2 nanosurfaces has also yielded promising results. Because of the toxicity and risk involved, experimental studies have been mostly confined to the benign simulants, whereas theoretical studies have attempted to compare the real agents with their mimics. These studies establish a qualitative correlation between the G-agents and their simulant DMMP, and, hence, decomposition on metal oxide surfaces can be analyzed by observing the surface chemistry of DMMP on a wide variety of metal oxide surfaces. This review attempts to compile the literature concerning CWA and their simulants.

Keywords: Chemical warfare agents; metal oxides; adsorption; simulants.

Neha Sharma is pursuing Ph.D in the Department of Chemistry, University of Delhi, after clearing the CSIR National Eligibility Test. She submitted her PhD thesis in January 2013. Her research interests include computational chemistry, and she has presented her work related to the computational study of chemical warfare agents at various conferences.

Rita Kakkar, after obtaining a PhD degree in Physical Chemistry from the University of Delhi, undertook research on various topics. She has been teaching physical chemistry at the University of Delhi for the past 28 years. Prior to that, she taught at Miranda House, University of Delhi. In the field of chemistry education, she is actively involved in designing syllabi of various universities and conducting teacher-training workshops, and for popularizing the use of Molecular Modelling in teaching chemistry. Her main research interests are in Computational Chemistry and related fields. She heads a large research group, which is carrying out computational and experimental studies on catalysis by nanomaterials and by enzymes. The focus of the research on nanomaterials is to understand the growth, morphologies and stabilities of nanocrystalline forms of metals and metal oxides, their reactivities, and their catalytic role in various reactions, particularly those involving degradation of organic pollutants. Her research on nanoscale materials also includes theoretical and experimental studies on quantum dots and their size-dependent properties for use as semiconductor devices and sensors. The other area of research is the use of *in silico* techniques to understand enzyme catalysis and to design enzyme inhibitors. Her group is presently engaged in understanding the action of PDHK, PDF and urease inhibitors in order to design better inhibitors by use of docking studies and structure-activity relationships. In addition, her research group investigates potential energy surfaces and reaction paths of important organic reactions, and studies the role of catalysts on these reactions. Prof. Rita Kakkar has over 80 research publications in international journals. She has successfully supervised the work of 27 PhD and 7 MPhil students. She has delivered invited several talks at scientific conferences. She acted as an International Advisory Member, First, Second, Third, Fourth, Fifth, Sixth and Seventh Workshops on Computational Chemistry and its Applications, part of the International Conference on Computational Science, ICCS: 2006, ICCS: 2007, ICCS: 2008, ICCS: 2009, ICCS: 2010, ICCS: 2011 and ICCS: 2012. She is also an International Advisory Member for the Eighth Workshop (8th CCA), part of ICCS 2013 to be held at Barcelona, Spain. She is a member, Task Force, IUPAC Project on "Assessment of theoretical methods for the study of reactions involving global warming gas species degradation and by-product formation". She also regularly reviews manuscripts for many international journals, including those published by the American Chemical Society, Royal Society of Chemistry and Elsevier.

Introduction

Chemical Warfare Agents (CWA) are intended in military operations to kill, seriously injure, or incapacitate people because of their physiological effects. They also contaminate the environment and ground water during their release, and thus the studies on the materials for the destruction and disposal of CWA are highly important.

The two major threat classes of these chemical weapons are sulfur mustard and the nerve agents. Sulfur mustard was used in World War I, and the nerve agents were developed shortly during, and after, World War II. These agents were designed to harm people by any route of exposure and to be effective at low doses. Sulfur mustard (**Fig. 1a**), bis-(2-chloroethyl)sulfide, also known as HD, S-mustard, HS, etc. smells like garlic or mustard, but its disabling vapor concentration may have so little odor that one is not aware of the danger until hours of exposure, when signs and symptoms begin to appear. Besides, it is colorless and tasteless, making it all the more dangerous as its detection by the senses is unlikely. HD has been recognized as a radiomimetic and a human carcinogen. On being absorbed inside the body, its toxic affects result from chemical reaction with the cellular constituents. These biochemical reactions cause inhibition of mitosis, nicotinamide adenine dinucleotide (NAD) depletion, decreased tissue respiration and ultimately death.

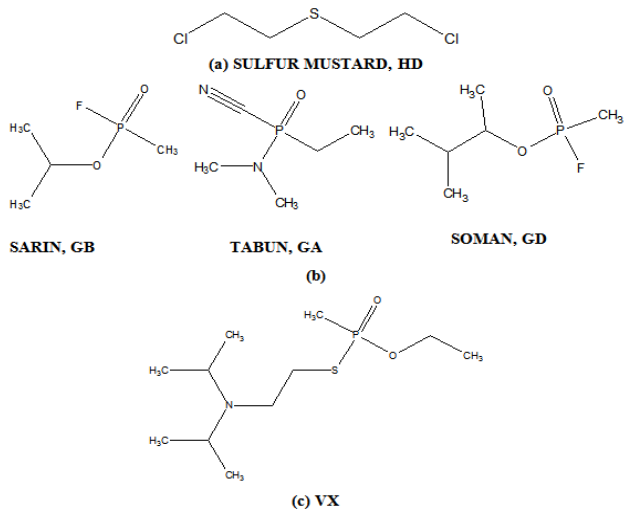

Fig. 1. Structure of (a) Sulfur mustard, (b) G-type chemical warfare agents, and (c) V-type chemical warfare agents.

Nerve agents are a subfamily of organophosphorus compounds developed for chemical warfare. Most of the nerve agents were originally synthesized in a search for insecticides, but because of their toxicity, they were evaluated for military use. They are generally grouped into two classes: G and V. G agents (**Fig. 1b**) are derivatives of phosphoramidocyanidic or methylphosphonofluoridate and include sarin (GB; isopropyl methylphosphonofluoridate), tabun (GA; ethyl N-dimethylphosphoramidocyanidate) and soman (GD; pinacolyl methylphosphonofluoridate). V agents (**Fig. 1c**) are derivatives of methylphosphonothioic acid. VX is primary V-type agent. Nerve agents are readily adsorbed by inhalation, ingestion, and dermal contact. The general properties of CWA are tabulated in **Table 1**.

Table 1. Properties of chemical warfare agents.

Name	Molecular Formula	Appearance	Molecular weight	Mode of Action	Decomposition Temperature	LD_{50} in rat oral (mg kg^{-1})[a]
HD	$C_4H_8Cl_2S$	Pale yellow to dark brown oily liquid with garlic odor	159.07	Vesicant	----	2.4
GA	$C_5H_{11}PO_2N$	Colorless to brown liquid giving off colorless vapors	162.12	Nerve Agent	423	1.06
GB	$C_4H_{10}PO_2F$	Colorless to brown liquid giving off colorless vapors	140.10	Nerve Agent	423	0.10
GD	$C_7H_{16}PO_2F$	Colorless to brown liquid giving off colorless vapors	182.20	Nerve Agent	403	*0.045
VX	$C_{11}H_{24}PO_2SN$	Amber colored Liquid	267.40	Nerve Agent	423	0.077-0.128

[a]*LD_{50} is lethal dose in 50%.*
**LD_{50} value for rat in vitro.*

The relative potencies of the CWA are VX > GD > GB > GA > HD, as evidenced by their LD_{50} values **[1-4]** given in Table 1. Because of the greater potency of the nerve agents, we briefly describe their mode of action on the nervous system.

Mode of action of nerve agents on the nervous system

The organophosphorus agents, or nerve agents, are often called "anticholinesterases", because they phosphoryle the enzyme acetylcholinesterase (AChE), which plays a significant role in the nervous system. Before going into the details of how nerve agents inhibit this enzyme, it is important to understand the role of this enzyme in the nervous system, which is explained below.

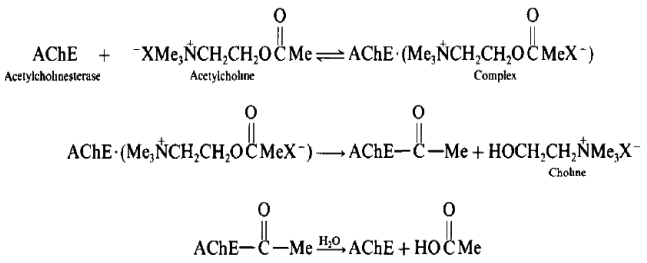

Fig. 2. Catalytic action of the enzyme acetylcholinesterase.

Signals are transmitted along nerve fibers by changing electrical potentials. When a muscle receives a signal from the brain, a neurotransmitter acetylcholine (in humans) is released at the end of the muscle fibers. It diffuses across the synapse (a gap of about 10^{-8} m between the nerve ending and muscle), causing a change in electrical potential on the muscle, thereby initiating muscular contraction. At this point, the enzyme AChE facilitates the hydrolysis of acetylcholine, producing products that no longer activate the muscle. This causes the muscle to relax. Therefore, each signal requires release and hydrolysis of acetylcholine, causing muscular contraction and relaxation many

thousands of times per second. The mechanism of acetylcholine hydrolysis (**Fig. 2**) is based on the formation of an initial complex with the enzyme, followed by release of choline, and hence hydrolysis of the esterified enzyme.

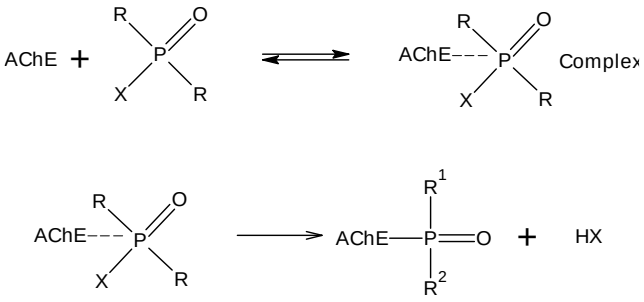

Fig. 3. Inhibition of acetylcholinesterase by chemical warfare agents.

Therefore, the inhibition of AChE caused by its phosphorylation by organophosphorous compounds renders the enzyme inactive, which forbids the transmission of nerve impulses, leading to failure of muscle movement. This results in an uncontrolled increase of acetylcholine concentration at cholinergic synapses, leading to a variety of cholinergic effects, such as myosis, salivation, hypotension, muscle tremors, convulsions and respiratory depression.

All organophosphorus pesticides and CWA of the general form $R^1R^2P(O/S)X$, where R^1, R^2 are alkyl or alkoxy groups and X is a good leaving group, are fairly good phosphorylating agents, because of the group X. These form stable complexes (**Fig. 3**) causing phosphorylation of the AChE enzyme and hence inhibit enzyme action **[5-7]**.

Role of chirality in inhibiting acetylcholinesterase

Interestingly, the chirality around the phosphorus atom has large implications for the toxicity of these agents. For these organophosphorus compounds, there exists a correlation between the biological activity and absolute and relative chirality. The existence of various stereoisomeric forms of nerve agents can be distinguished in NMR spectroscopy by the use of chiral shift reagents **[8-9]**. For GD, its four stereoisomers have been separated and were found to differ in anticholinesterase activity by up to 105-fold, and in acute toxicity by up to 100-fold from the least toxic to the most **[10]**. The absolute configuration **(S)-(-)** at the chiral phosphorus center for the most active forms has been determined from analysis of NMR coupling constants of the two diastereomeric forms of GD **[11]**. On the basis of chemical correlation, the same absolute **(S)-(-)** configuration was proposed for the more toxic enantiomer of GB **[10]**. The conformational properties of GA indicate the presence of two enantiomers (R and S). These two enantiomers have been isolated **[12],** and it has been found through crystallographic studies **[13]** that the S enantiomer accounts for the AChE inhibition property of this molecule. The R form is almost inactive.

The CWA were used in the World Wars, in terrorist attacks against Japan (1984 and 1985), and in the Iran-Iraq war in the 1980s, killing and injuring a large number of people. Therefore, with the push towards demilitarizing chemical weapons, as well as the importance of quickly detecting and decomposing CWA employed against troops and civilians, research on reactivity of CWA and their detoxification is important.

Reactive decontaminants for chemical destruction of CWA have been characterized by their capability to neutralize CWA in a rapid and safe manner, ease of handling, stability in long-term storage, environment friendliness, availability, and easy disposal. Extensive research over decades has established that metal oxides possess all the above mentioned characteristics and hence have been exclusively exploited for decomposition of CWA.

Decomposition of chemical warfare agents on metal oxides

Metal oxides demonstrate superior ability to adsorb and decompose CWA compared to pure metal surfaces. This is often attributed to reactive sites on the metal oxide surface through which organophosphonate species (nerve agents) can adsorb and subsequently undergo a hydrolysis reaction. A wide variety of metal oxide systems have been studied, from clean, crystalline surfaces to high surface area nanomaterials. Metal oxides, well known for their industrial use as adsorbents, catalysts and catalyst supports, have several potential decontamination applications such as environment friendly hasty decontamination on the battlefield, protective filtration systems for vehicles, aircraft, and buildings, and the demilitarization of CWA munitions and stockpiles. In contrast to their conventional counterparts, nanoscale metal oxides possess significantly different properties and have been established as the potential adsorbent materials for decontamination of CWA.

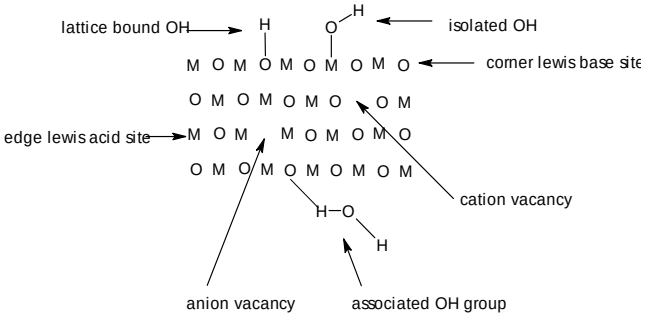

Fig. 4. Reactive sites on surface of metal oxides.

Due to their high surface area, large number of highly reactive edges, corner defect sites, unusual lattice planes and high surface to volume ratio, nanocrystalline metal oxides possess enhanced reactive properties towards CWA **[14-16]**. **Fig. 4** demonstrates reactive sites, such as Lewis acid (metal cations), Lewis base (oxide anions) and defect sites (Frenkel & Schottky) available on the surface of metal oxides, particularly on nanoparticles, which contribute to their reactivity towards CWA. Thus, metal oxides, such as MgO **[17-18]**, CaO **[19-20]**, Al_2O_3 **[21-25]**, TiO_2 **[26-35]**, ZnO **[36-38],** etc., are currently under consideration as destructive adsorbents for decontamination of CWA. The term "destructive adsorbent" refers to the ability to efficiently adsorb and, at the same time, to chemically

destroy incoming adsorbate. In the next section, various metal oxides and their role as destructive adsorbents are explored.

Magnesium oxide (MgO)

Nanoparticles of MgO exhibit novel surface chemistry and possess reactive surface due to the presence of defects and low-coordinated sites. Researchers found that, in nanocrystalline MgO, 30-40% of the MgO moieties are on the surface, providing high surface area, which allows adsorption and simultaneous destruction of toxic chemicals **[39-40]**.

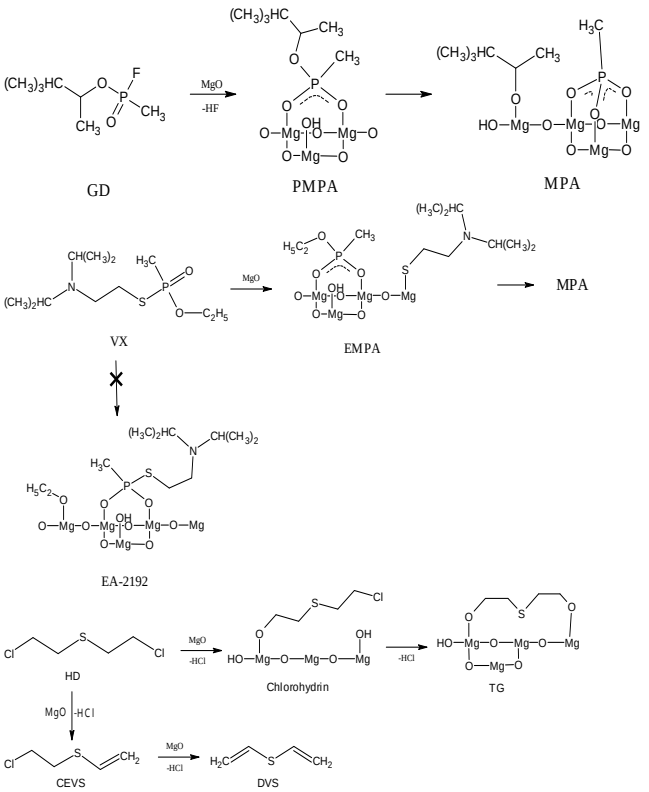

Fig. 5. Decomposition of GD, VX & HD on MgO nanoparticles.

The highly reactive surface properties of MgO nanoparticles prompted researchers to use it for the decomposition of toxic organophosphorus compounds. Wagner and co-workers **[18]** carried out an experimental study on the hydrolysis reactions of three CWA, namely VX, GD and HD, on the surface of MgO nanoparticles, and characterized the products by solid-state Magic Angle Spinning (MAS) NMR. The reaction mechanism, shown in **Fig. 5**, reveals that the hydrolysis reactions are quite similar to those observed in solution **[41]**, except that the resulting products form non-toxic surface-bound metal phosphonates (VX and GD) and metal alkoxides (HD). Owing to surface hydroxyls and physisorbed water on the MgO surface, VX yields ethyl methylphosphonic acid (EMPA) and methylphosphonic acid (MPA), but no toxic *S*-(2-diisopropylamino) ethyl methylphosphonothioate (EA-2192), which was observed for basic hydrolysis of VX in solution **[42-43]**. GD forms pinacolyl methyl phosphonic acid (PMPA) and MPA. For VX and GD, broad ^{31}P NMR lines observed for their products are consistent with the formation of surface-bound magnesium phosphonates. In case of HD, both hydrolysis and elimination reactions, characterized by ^{13}C NMR, are the preferred hydrolysis pathways. The former yields thiodiglycol (TG), whereas in the latter, 2-chloroethyl vinyl sulfide (CEVS) via HCl elimination was obtained initially. CEVS subsequently undergoes a second HCl elimination to yield divinyl sulphide (DVS). The final product ratio is about 50% TG and 50% DVS, which are not surface bound due to lack of any binding interaction with the surface and remain volatile **[18]**.

To understand the experimental work in a better way, Michalkova and co-workers **[17]** investigated the decomposition mechanism of GB on MgO nanoparticles theoretically. For this, $Mg_{16}O_{16}$ and Mg_4O_4 cluster models were developed to study the dependence of the adsorption ability on cluster size. Adsorption of GB on the $Mg_{16}O_{16}$ model resulted in some redistribution of the electron density, associated with an internal polarization. Their calculations showed that GB is adsorbed on $Mg_{16}O_{16}$ via molecular physisorption, which was attributed to the creation of hydrogen bonds and to ion-dipole and dipole-dipole interactions between GB and the surface. On the other hand, the adsorption results for small cluster model (Mg_4O_4) were found to be more characteristic of chemisorption, owing to formation of covalent bonds between the surface and GB. In this case, the formation of three covalent bonds (between P(GB) and O(cluster), phosphoryl O(GB) and Mg(cluster), and alkoxy O(GB) and Mg(cluster)) has been reported for the energetically most favorable complex. The superior reactivity of small clusters owing to irregular edges, corners and defect sites was thus demonstrated.

The authors also performed hydroxylation of the small cluster model to contrast the reactivity of hydroxylated and unhydroxylated nanocrystal surfaces. The unhydroxylated-GB complex was found to be more stabilized as compared to the hydroxylated-GB complex, owing to the larger number of covalent bonds formed between GB and the surface. The unhydroxylated surface of MgO resulted in decomposition by transfer of the F atom from GB to an Mg ion on the surface, while HF was formed on hydroxylated MgO fragments. This work provided the rationale for the superior reactivity of unhydroxylated small clusters of nanomaterials.

Calcium oxide (CaO)

The well-known adsorption properties of CaO towards acid gases, such as SO_2, polar organics etc. makes it a good candidate for adsorption of organophosphorus compounds. Wagner *et al*. **[20]** carried out an experimental study on the decomposition of CWA on the CaO nanosurface, in line with their previous work on MgO **[18]**. The hydrolysis reactions for GD and VX on CaO were found to be consistent with those observed on MgO. VX and GD hydrolyze to yield surface-bound complexes of nontoxic ethyl methylphosphonate (EMPA) and pinacolyl methylphosphonate (PMPA), respectively. For VX and GD, broad ^{31}P MAS NMR lines observed for their products are consistent with the formation of surface-bound calcium phosphonates.

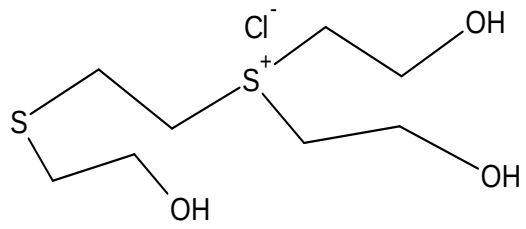

Fig. 6. Structure of CH-TG (sulfonium ions such as CH-TG result from the reaction of CH (chlorohydrin) and TG (thiodiglycol) hydrolysis products).

In contrast to the 50:50 product distribution ratio observed on MgO **[18]**, the product distribution for HD on CaO was about 80% divinyl sulfide and 20% thiodiglycol and/or sulfonium ions (CH-TG) (**Fig. 6**), which apparently reside as surface alkoxides. On partially hydrated CaO, a rather fast steady-state elimination of HCl was observed owing to acid-catalyzed surface reconstruction (to regenerate fresh surface) and the formation of $CaCl_2$, which is known to be more reactive than CaO. **Fig. 5** for the mechanism for the decomposition of GD, VX and HD on the surface of MgO applies to CaO as well, with only one exception, the formation of sulfonium ions as competing reaction in case of HD.

In another theoretical work, intended to facilitate a more extensive understanding of the interactions of nerve agents with metal oxides nanoparticles **[19]**, the studied adsorbent CaO was characterized for efficient detection and disposal of the nerve agent GA. The non-hydroxylated Ca_4O_4, partially hydroxylated $Ca_4O_4(OH)H$ and hydroxylated $Ca_4O_4(OH)_2H_2$ models were designed to mimic the calcium oxide surface. The calculated interaction energies, -87.8 kcal mol^{-1}, -27.4 kcal mol^{-1} and -26.7 kcal mol^{-1}, respectively, for the Ca_4O_4-GA, $Ca_4O_4(OH)H$-GA and the $Ca_4O_4(OH)_2H_2$-GA systems, reveal the formation of a much more stable complex on the unhydroxylated (Ca_4O_4-GA) system. The complex formation is stabilized by covalent bonding between the P atom of GA and the cluster oxygen atom (chemisorption), resulting in the decomposition of CWA **[17]**. On the other hand, the geometrical and topological parameters for the hydroxylated and partially hydroxylated CaO complexes indicate weaker and competitive hydrogen bond interactions, because of the larger coordination of both the surface oxygen anion site and the Ca cation site, which reduces their reactivity, supporting molecular physisorption. The result is, however, in contrast to an experimental study on the CaO surface **[20]**, which reported that the presence of water seems to benefit the decomposition process.

The strong interaction of the P=O bond with the cluster indicates that the nonhydroxylated complex could be useful for the hydrolysis of GA, while the weakly bound partially hydroxylated and hydroxylated complexes are useful for GA detection.

Aluminium dioxide (Al_2O_3)

γ-Al_2O_3 is of interest as a solid adsorbent **[44,45]** for air purification or as a catalyst support **[46]** in the chemical destruction of CWA. Preliminary work examining the interaction of the chemical warfare agent GB on γ-alumina was published by Kuiper *et al*. **[21]**. They observed that GB adsorbs through the phosphoryl oxygen on the Lewis acid sites present on the surface. Hydrolysis of the P-F bond was found to occur in addition to dealkylation that liberated propene. Fluorine remained on the surface after hydrolysis, in addition to an O-P-O bridging species. Adsorption of HF inactivated the surface, whereas the addition of water accelerated the reaction.

Wagner *et al.* **[25]** next took up Al_2O_3 nanoparticles for their study of the hydrolysis reaction of liquid VX, GB and GD on metal oxide nanoparticle surfaces. Their results indicated that nerve agents hydrolyze to yield surface bound complexes of their corresponding nontoxic phosphonates, whose restricted mobility on the Al_2O_3 surface was confirmed by broad ^{31}P MAS NMR peaks.

For VX and GD, the innocuous products obtained on hydrolysis were the same as those obtained on MgO and CaO **[18,20]**. GB was converted to the non-toxic isopropyl methylphosphonic acid (IMPA). The surface-bound phosphonic acid hydrolysis products are converted to aluminophosphonate complexes, causing facile erosion of the alumina surface, and exposing new surface for adsorption of the nerve agents. Thus, the reactive capacity can be exceedingly large for the nerve agents at sufficiently high loadings, since the reaction can continue to the core of the alumina nanoparticles, instead of being limited to the surface. This implies that the alumina surface is more reactive than the corresponding MgO and CaO surface, although reaction with VX and GD yields similar non-toxic metal phosphonates in all three cases. In case of HD, the hydrolysis products are thiodiglycol (TG, 71%) and a small amount of the CH-TG sulfonium ion (12%), accompanied by elimination of HCl (17%).

Saxena *et al*. **[22,23]** employed Al_2O_3 nanoparticles impregnated with various chemicals to study the decontamination of sulfur mustard and the kinetics involved in its adsorption. The following year, the same research group **[24]** studied the decomposition of GB over Al_2O_3 nanoparticles and demonstrated its detoxification to IMPA.

Zinc oxide (ZnO)

ZnO has long been known as a catalyst, adsorbent, toxic gas sensor, etc. **[47-50]**. It has been found to be a promising adsorbent for the degradation of environmental pollutants, both in normal and light irradiated conditions. Its reactivity towards toxic chemicals under normal conditions has been attributed to the presence of Lewis acid, Lewis base, and Brönsted acid sites of varying coordination, and also to surface hydroxides **[47,49,51-52]**. Moreover, the photocatalytic property exhibited by ZnO nanomaterials plays an interesting role in the photocatalytic decontamination of persistent CWA **[36]**. These properties attracted research interest for detoxification of CWA on the surface of ZnO nanoparticles **[36-38]**.

ZnO nanorods, a variant of nanomaterial, are known to possess sensing **[53]** and catalytic properties **[54]**, which highlight their role as effective decontaminating agents. Prasad *et al*. **[37]** used ZnO nanorods as adsorbents for HD decomposition, and compared their results with those obtained for bulk ZnO. Although they did not find much difference in the respective surface areas, ZnO nanorods showed higher rate of destructive reaction owing to the

presence of a larger number of reactive sites in the form of defects and surface hydroxyls, though they have less moisture content than the bulk. Gas chromatography-Mass spectrometry (GC-MS) data indicated formation of thiodiglycol (TG), hemi-sulfur mustard, confirming the role of the hydrolysis reaction (**Fig. 7**), and chloroethyl vinyl sulfide (CEVS), divinyl sulfide (DVS) and hydroxyethyl vinyl sulfide (HEVS), confirming the role of the elimination reaction (**Fig. 8**) in decontamination of HD. The hydrolysis pathway was found to yield similar products to those recorded by Wagner *et al*. **[18,20]** on MgO and CaO, whereas the elimination pathway presented different reaction products. Both pathways proceeded with formation of sulfonium ions.

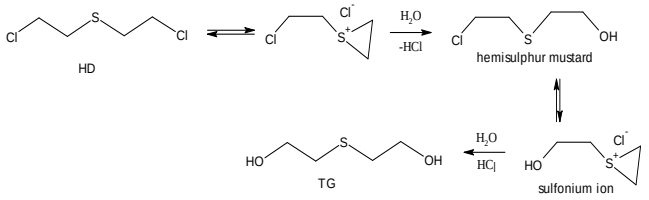

Fig. 7. Hydrolysis reaction of HD on ZnO nanorods.

Further, in order to examine the effect of light on the decontamination properties of ZnO nanoparticles, the same research group **[38]** then carried out sunlight assisted photocatalytic decontamination of sulfur mustard (HD), and compared the data with the reaction carried out in the presence of UVA and visible light radiation. It was seen that in the presence of sunlight, 100% of HD was decontaminated in 12 h, whereas in the presence of UVA light, 90%, and in visible light, 80% of HD was decontaminated in 12 h. For the experiments carried out in the dark and under visible light irradiation, GC–MS data indicated the formation of thiodiglycol, hemisulfur mustard, divinyl sulfide, 2-chloro ethyl vinyl sulfide, etc., on the surface of ZnO nanoparticles. However, in sunlight and UVA light irradiation experiments, GC–MS data indicated the formation of HD sulfoxide, HD sulfone, 1,3-dithiane, 2-chloro ethanol, acetaldehyde, carbon dioxide, etc. along with hydrolysis and elimination products. While the credit for decontamination of HD in the dark and under visible light was given to elimination and surface complexation reactions, photocatalytic reactions like C–S bond cleavage, oxidation of C, S atoms, in addition to the hydrolysis and elimination reactions, contribute to decontamination of HD in the case of sunlight and UVA light.

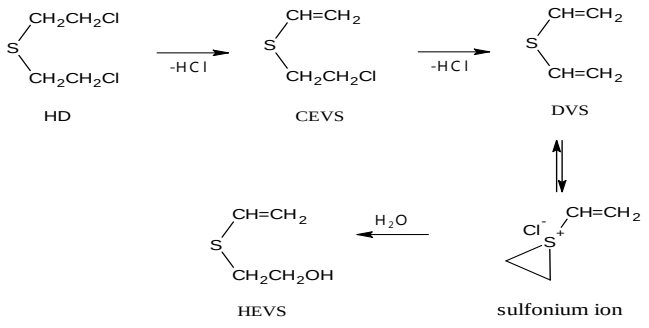

Fig. 8. Elimination and hydrolysis reactions of HD on ZnO nanorods.

Inspired by the work carried out by Prasad *et al*. **[37]**, Mahato *et al*. **[36]** synthesized ZnO nanomaterials by the sol-gel method and studied the decontamination reactions of GB on the surface by Gas Chromatography. They obtained similar results regarding the higher rate of decontamination on the surface of the nanomaterial as compared to the bulk. The surface hydroxyls in ZnO nanomaterials attack the P-F bond, and GB is converted initially to isopropyl methylphosphonic acid (IMPA) and further into methyl phosphonic acid (MPA) (**Fig. 9**), which exists both in surface bound and free states, as evidenced by IR data. The above experimental results showed that the adsorption behavior of ZnO nanomaterials is comparable to that of other solid decontaminants, such as nano-sized MgO, Al_2O_3, etc.

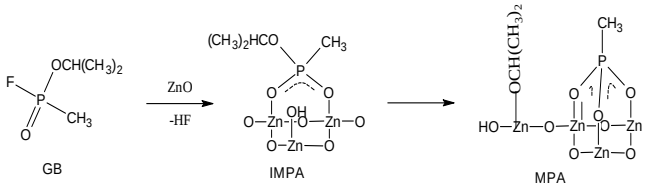

Fig. 9. Hydrolysis reactions of GB on the surface of ZnO nanomaterials.

Titanium dioxide (TiO_2)

A limitation to the broad spectrum reactivity of nano metal oxides such as MgO, CaO, and Al_2O_3 is their instability in the presence of air and/or moisture. Titania, on the other hand, shows exceptional stability, allowing it to even pass through the human digestion intact and thus is also used in food items.

As far as the nanocrystals or nanoparticles are concerned, their tendency to aggregate limits the number of available active sites on the surface. Nanotubes (NTs), on the other hand, aggregate without losing their surface area, making them more accessible to adsorbate molecules.

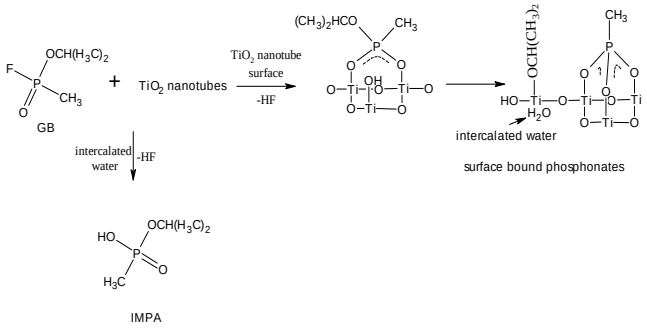

Fig. 10. Decontamination reactions of GB on TiO_2 nanotubes.

The decomposition of HD and GB on TiO_2 nanotubes in the powder form has been studied **[28,29,34]**, and found to proceed faster on the surface of TiO_2 NTs than on the surface of bulk material **[28]**. The higher surface area (271 $m^2\ g^{-1}$) for NTs as compared to the bulk material (40 $m^2\ g^{-1}$) ensures that a larger amount of CWA is adsorbed on the NTs surface and reacts with the relatively larger number of reactive sites available on TiO_2 NTs. GB and HD

molecules react with NTs in two ways (**Fig. 10** and **Fig. 11** respectively):

1. They react with intercalated or physisorbed water molecules present on the surface of NTs to form isopropyl methylphosphonic acid (IMPA; in case of GB) and thiodiglycol (TG; in case of HD).
2. They react with isolated hydroxyl groups (Ti-OH) and Lewis acid (Ti^{4+}) sites to form surface bound alkoxy species.

The cyclic sulfonium ion, initially formed in the case of HD, could not be detected by GC since it is in the nonvolatile form of a salt **[20,55]**.

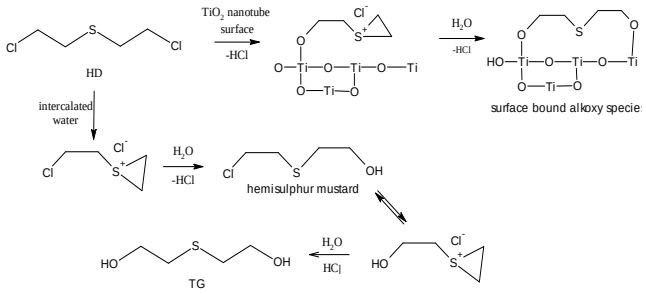

Fig. 11. Decontamination reactions of HD on TiO_2 nanotubes.

The authors then modified the TiO_2 NT, using transition metal ions such as Ru^{3+}, Ni^{2+}, Cu^{2+}, Ag^{+}, Mn^{2+}, and Co^{2+} **[29]**. The rate of decontamination of HD was found to increase on the surface of Ag^{+}-TiO_2 with respect to the original TiO_2 nanotube, because of the abstraction of the chloride ion by Ag^{+}. Other materials (Ru^{3+}, Ni^{2+}, Cu^{2+}, Mn^{2+}, Co^{2+}-TiO_2 NTs), however, exhibited lower rate constants than even the original TiO_2 NTs, indicating their negligible role in abstraction of the chloride ion.

The decomposition reactions of VX, GD and HD on nanotubular titania (NTT) **[34]** proceeds by the hydrolysis of all three agents, the reaction of VX being profoundly fast, approaching the rate achievable with liquid decontaminants. VX is adsorbed within the NTT tubules and/or its titania layers, as confirmed by ^{31}P MAS NMR. Comparison with conventional titania (anatase) for the VX decontamination reaction revealed that anatase hydrolyses VX faster than other metal oxides, but is slower than NTT. For HD and GD, the availability of abundant water efficiently promoted their hydrolysis to CH-TG sulfonium ion and pinacolyl methylphosphonic acid (PMPA; surface bound), respectively.

Studies of the adsorption and photocatalytic decomposition of GB on the surface of the TiO_2 photocatalyst **[26,31]**, revealed that the initial products are the same as in the non-photocatalytic reactions, but the final product is phosphoric acid formed by the complete degradation of GB, according to the equation:

$$C_4H_{10}PO_2F + 13/2\ O_2 + TiO_2 \rightarrow H_3PO_4 + 4CO_2 + 3H_2O + F/TiO_2$$

The fact that GB is quickly mineralized to phosphoric acid, CO_2 and H_2O implies that photocatalysis can serve as an effective decontamination system.

The photocatalytic decomposition of HD was studied in the absence and presence of TiO_2 nanoparticles **[27]**. While 90% destruction of HD was observed in 6 h in the absence of TiO_2, complete destruction occurred in just 3 h in its presence. The degradation products, as identified by the GC-MS technique, were identical to those found in previous experimental studies on HD. However, in the absence of irradiation, no degradation product was observed in 3 h. The photocatalysis by nano-TiO_2 presented better results than those obtained for nano-ZnO **[38]** as a photocatalyst for HD decomposition. In another experiment **[30]**, similar results were obtained for the photocatalytic HD decontamination on the TiO_2 nanosurface, and only 24.7% decomposed in the absence of irradiation. In the former case, GC–MS data indicated decontamination of HD to acetaldehyde, carbon dioxide, sulfur mustard sulfoxide, thiodiglycol, acetic acid, etc., while in the latter, only the hydrolysis products of HD, like thiodiglycol, were observed.

Vanadia (V_2O_5)

Non-stoichiometric vanadia ($V_{1.02}O_{2.98}$) nanotubes also possess decontamination properties against CWA **[56]**. Hydrolysis reactions on the surface of $V_{1.02}O_{2.98}$ nanotubes and formation of surface bound alkoxy species and surface bound phosphonates facilitate decontamination of HD and GB, respectively, and render them non-toxic. The reactions proceed by the same mechanism as in the case of TiO_2 nanotubes **[28]**, but the reaction is slower.

Clay Minerals

Recently, a lot of interest has been centered on studying the adsorption properties of clay minerals (layered aluminosilicates that consist of a continuous sheet of corner sharing tetrahedra bound to parallel sheets of edge sharing metal octahedra) which can be considered as natural adsorbents. These layered aluminosilicates demonstrate a large variety of important physicochemical properties: sorption ability, large specific surface, ability to intercalate or to exchange ions and molecules, catalytic properties and surface acidity **[57,58]**. Therefore, clay minerals are used as natural adsorbents and catalysts in industrial applications for the purification and recycling of water systems, disposal of radioactive elements from water, remediation of explosive contaminants and several other applications **[59,60]**. Thus, the large sorption ability of clay minerals prompted researchers to study these for disposal of nerve gases **[61,62]**.

Although basal surfaces of clay minerals are characterized exclusively by charge-saturated and extremely stable siloxane bonds, the reactivity of such surfaces can be attributed to the presence of defects. These defects arise when polar covalent bonds between the oxygen atoms and central cations of the tetrahedral sheets are broken. These partially coordinated oxygen anions have the tendency to bind strongly with protons, resulting in the formation of surface hydroxyls. Apart from surface hydroxyls, edge OH groups also play a considerable role, since they increase the electronegativity of clay minerals and hence their capacity to adsorb cations.

The known reactivity of silica surfaces prompted theoretical studies of the interaction of phosphate with silica and hectorite **[63,64]**, which confirmed the efficacy of clay minerals as decontaminants. The interactions of GB and GD with dickite, a typical representative of minerals of the kaolinite group with a dioctahedral 1:1 layer structure consisting of an octahedral aluminum hydroxide sheet and a tetrahedral silica sheet **[57,58]**, have been investigated **[61]**. The authors employed two cluster models to mimic the surface of dickite. The active sites for adsorption on the clay minerals are the hydroxyl groups of the octahedral side and the oxygen atoms of the Si-O-Si groups on the tetrahedral side, which form hydrogen bonds with GB and GD. The size of the cluster was found to have negligible effect on the adsorption energies, but the interaction energies were found to be more negative for adsorption at the octahedral site than at the tetrahedral site.

The edge structures of clay are much more reactive than the basal surfaces, as has been experimentally demonstrated **[65]**. This is attributed to broken bonds and their well-known tendency to form inner-sphere complexes with protons and other cations **[65-69]**. A study of the interaction of GB and GD with tetrahedral edge clay mineral surfaces containing the Al^{3+} or Si^{4+} central cations (the $[AlO(OH)_3]^{2-}$, $[Al(OH)_4]^-$, $Si(OH)_4$, and $[SiO(OH)_3]^-$ fragments) **[62]** led to the conclusion that the adsorption on the neutral complex is characterized by the formation of weak C-H…O and O-H…O hydrogen bonds, resulting in physisorption. However, in the case of charged clusters, chemisorption occurs, owing to formation of a chemical bond between a phosphorus atom of GB/GD and an oxygen atom of the charged clusters.

The thermodynamic parameters also show some interesting aspects. The calculated Gibbs energy values for the adsorbed system were found to be negative only in case of the charged edge mineral fragment with an Al^{3+} central cation, highlighting its thermodynamic stability. Interaction energy results also indicated that the strongest adsorption of GB and GD is for a (-2) charged $[AlO(OH)_3]^{2-}$ mineral fragment, where the P-O covalent bond is created, and the interaction energy is much higher than that observed on dickite **[61]**. Therefore, it can be concluded that GB and GD are adsorbed preferably on charged edge mineral surfaces containing Al^{3+}, than on regular electroneutral mineral surfaces.

Chemical warfare agent's simulants

The high toxicity of CWA is a major hindrance to any study on the uptake and reactivity of the agents with surfaces. In addition, the varied functionality of the nerve agents makes it difficult to isolate the role of each functional group in the overall chemistry of the molecules. For these reasons, CWA simulants are employed by both the military and academic researchers.

A simulant is considered ideal if it mimics all significant chemical and physical properties of the agent without its associated toxicological properties. Although a number of compounds have been used as CWA simulants (Table 2), no specific compound is ideal because a single simulant cannot adequately represent all environmental fate properties of a given CWA. Thus, depending on the concerned physical-chemical property, a number of different chemicals are used as chemical warfare agent's simulants.

Simulants classification

The structures of various (commonly used) simulants are depicted in Table 2, along with their available Lethal Dose (LD_{50}) values **[70-77]**.

Sulfur Mustard (HD) Simulants

Innumerable compounds have been used to simulate HD. Chloroethyl ethyl sulfide (CEES) or half mustard (HM) is the most common simulant, and was used to simulate HD in a study of CWA removal from water using activated carbon filters **[78]** and to study its hydrolysis reaction **[79]**. The other important simulants, 2-chloroethyl methyl sulfide (CEMS) and 2-chloroethyl phenyl sulfide (CEPS) were used for studying the degradation and fate of HD in soil **[80,81]**.

G-Agent Simulants

A number of potential simulants for the three G-agents; GA, GB, and GD have been identified. Diphenyl chlorophosphate (DPCP) was used as a simulant for G agents in order to examine detoxification via oxidation **[82]**. In a study pertaining to the evaluation of the adsorption of G agents on the components of a furnished room, three simulants, dimethyl methylphosphonate (DMMP), diethyl ethylphosphonate (DEEP) and triethylphosphate (TEP) were used **[83]**. Diisopropyl methylphosphonate (DIMP) was used to examine the sorption of organic contaminants from water by activated carbon fibers **[78,84]**, and DMMP and TMP were studied to simulate the decomposition reactions of G type CWA on metal oxide surfaces **[85-87]**.

V-Agent Simulants

Amiton (VG) has been commonly used to simulate VX **[82,88]**. However, it exhibits many of the toxic properties of VX. Additionally, *O,S*-diethyl phenylphosphonothioate (DEPPT) and organophosphorus pesticides, such as malathion and parathion, have been used to simulate VX **[81,89-91]**. The LD_{50} values for various simulants (**Table 2**) show that they exhibit lower toxicity than their real agents (**Table 1**). Also, it can be seen that DMMP has the highest LD_{50} value, which makes it the best simulant, and has, therefore, been the most employed simulant for research.

Dimethyl methylphosphonate (DMMP)

DMMP is frequently used as a simulant molecule for understanding the activity of the organophosphorus nerve agents (G-agents), since it is nontoxic and exhibits structural similarities to the nerve agents. Moreover, DMMP exhibits many of the group frequencies associated with the actual agents in infrared spectroscopy, making it ideal for evaluating infrared methods of nerve agent detection **[92]**. Although it is not classified as toxic, it is harmful if inhaled, swallowed, or absorbed through the skin.

Table 2. CWA simulants: structure and available LD_{50} values.

S.No.	Simulant	Type	Structure	LD_{50} in rat oral (mg/kg)	Ref.
1	CEES/HM	HD	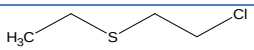	*566	[70]
2	CEMS	HD	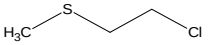	-	
3	CEPS	HD	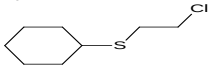	-	
4	DPCP	G agent	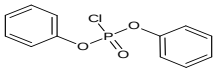	-	
5	DMMP	G agent	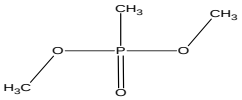	8210	[71]
6	DEEP	G agent	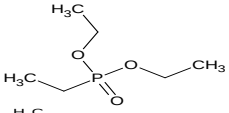	-	
7	TEP	G agent	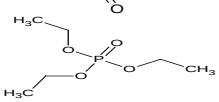	1600	[72]
8	DIMP	G agent	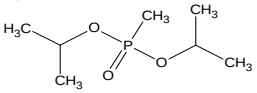	826	[73]
9	TMP	G agent	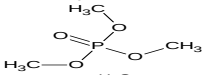	840	[74]
10	Amiton	V agent	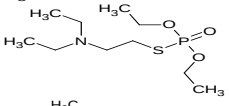	3.3	[75]
11	DEPPT	V agent	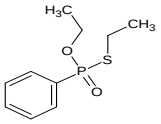	-	
12	Malathion	V agent	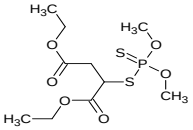	290	[76]
13	Parathion	V-agent	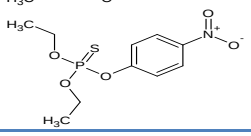	2	[77]

*LD_{50} in mice oral.

Experimental studies on DMMP decomposition

The adsorption and decomposition of DMMP on bulk oxides has been reported for WO_3 **[54,93-94]**, Fe_2O_3 **[95-97]**, MnO_2 **[98]**, TiO_2 **[54,94,99-105]**, Al_2O_3 **[21,54,97,106,107-109]**, La_2O_3 **[97]**, SiO_2 **[96,106,110-114]**, and MgO **[54,97,115,116]**. Additionally, the interaction of DMMP with nickel, iron, copper, vanadium, and cerium oxides, supported on α-Al_2O_3 **[107,117-119],** and on titania-supported nickel and copper metal clusters **[120-121]** has been studied.

DMMP interaction with metal-oxide nanomaterials has been studied with MgO **[122-123]**, CaO **[124]** and Y_2O_3 nanoparticles **[85]** and with heterogeneous CaO **[124]**, MgO **[125-126]**, TiO_2 **[127-129]**, Pt activated ZnO **[130]** and CeO_x **[118,131]** nanocomposites and thin films, confirming enhanced reactive properties for the nanomaterials. The adsorption chemistry of DMMP on metal oxides resembles that of the real agents. As demonstrated in **Fig. 12**, DMMP readily adsorbs through the phosphoryl oxygen onto most metal oxides at Lewis acid (metal atom) or at Brönsted acid (hydroxyl) sites **[97,123]**. The decomposition on metal oxides (excluding silica) occurs via oxidation or hydrolysis on the surface.

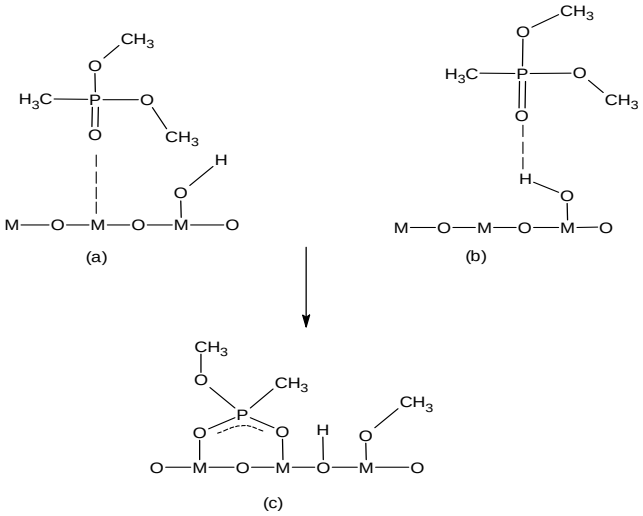

Fig. 12. Proposed structure of (a) molecular DMMP adsorbed at a Lewis acid site, (b) molecular DMMP adsorbed at a Brönsted acid (hydroxyl) site, and (c) dissociated DMMP along with a surface-bound methoxy group.

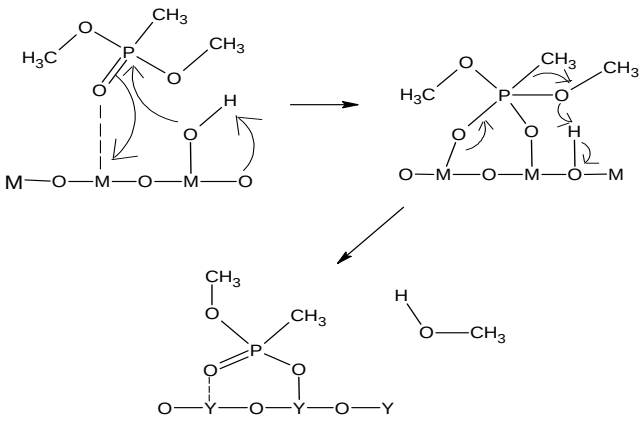

Fig. 13. Mechanism involved in DMMP decomposition.

The mechanism of interaction (**Fig. 13**) on the MgO, Al_2O_3, Y_2O_3, La_2O_3 and WO_3 surfaces, as envisaged by the above mentioned research groups, suggested that, at first, DMMP is adsorbed molecularly through the phosphoryl oxygen to the surface at an acid site (generally metal cation), followed by stepwise elimination of the methoxy group. This methoxy group subsequently combines with surface hydrogen atoms to yield methanol, which, being volatile, is evolved from the surface. Finally, a surface-bound methyl phosphonate product is observed, with the P-CH_3 bond intact. The formation of surface bound PO_x species poisons the active sites from future reaction **[54,93,94,97,107-109,115,116]**.

In general, room temperature decomposition of DMMP has been observed for a few metal oxide materials **[107,109]**. While experimental studies **[18,20,25]** in case of real agents highlighted the leading role played by water and

the hydroxyl group, their role in determining the outcome of the DMMP–metal oxide encounter is not completely understood.

Catalysts play a predominant role in increasing the surface activity of metal oxides **[125]**, as observed in the case of Fe_2O_3 and V_2O_5 catalysts coated on MgO and CaO in the decomposition of DMMP. The catalytic effect was attributed to the intermediacy of transition metal phosphates, which are mobile and seek out reactive sites on MgO and CaO.

The O-CH_3 bond is preferentially attacked, unless an alternative mechanism is available, for oxides like manganese oxide **[98]**, alumina-supported cerium oxide and iron co-impregnated oxide **[132]**, cerium oxide, Fe_2O_3, silica **[96,110,118,119]** and TiO_2 **[101,102,104,133]**. However, the adsorption of DMMP on SiO_2 **[110-111]** is remarkably different from that on WO_3, TiO_2 and Al_2O_3 **[97,104,111,114]**. While decomposition via elimination of methoxy groups has been reported for WO_3, TiO_2 and Al_2O_3, weak interaction via formation of two hydrogen bonds between DMMP and the surface hydroxyls on SiO_2 has been reported for high surface area SiO_2 powders (**Fig. 14**). However, at sufficiently high temperatures, complete molecular desorption occurs from the SiO_2 surface. Auger electron spectroscopy (AES) has been used **[96]** to analyze the interactions of DMMP with SiO_2. For dehydrated SiO_2, no decomposition of DMMP was observed, while on the hydrated surface about 10% DMMP decomposed into methylphosphonate and methanol.

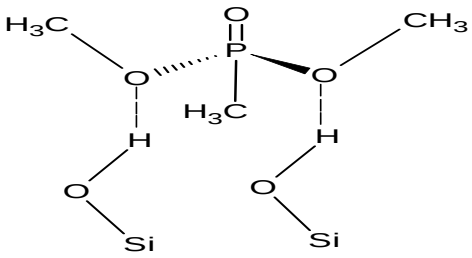

Fig. 14. DMMP adsorbed on SiO_2 through hydrogen bonding.

On amorphous manganese oxide and Al_2O_3-supported manganese oxide catalyst, the decomposition of DMMP was found to occur via thermal oxidation to CO_2 **[98]**, but on alumina-supported cerium oxide, the products are methanol and dimethyl ether **[118]**. Adsorption of DMMP on the iron oxide surface takes place via cleavage of the strong phosphorus-carbon covalent bond **[119]**. This phenomenon has been attributed to the availability of multiple oxidation states to the Fe atom, which allows participation of the Fe(III)/Fe(II) redox couple in the reaction, providing a low-energy path for oxidative cleavage of the P-CH_3 bond. Such kind of behavior is not possible for other metal oxides, which cannot provide a similar path of decomposition, and hence, the P-CH_3 bond remains intact.

The well-known photocatalytic property of TiO_2 allows the decomposition to proceed via a different pathway. Therefore, other than the usual decomposition mechanism via cleavage of P–OCH_3 groups **[103,105]** with the production of Ti–OCH_3 surface species, photodegradation of DMMP in a stepwise manner also occurs to give methylphosphonic acid, PO_4^{3-}, H_2O and CO_2 as products **[101,102,104,133]**.

Theoretical studies on DMMP decomposition

In order to develop a better understanding of the experimental work concerning decomposition of DMMP on metal oxides and the mechanisms involved, various theoretical models have been designed. For interaction with CaO nanoparticles, it was found **[86]** that the adsorption mechanism for CaO-DMMP and CaO-TMP systems is analogous to the previously studied CaO-GA system **[19]**, with the only difference that, in this case, chemisorption occurs even on the partially hydroxylated system. The authors also concluded that stabilization of DMMP on CaO cluster models is greater than that of GA (order of 2 kcal mol^{-1}), and that DMMP is a better simulant than TMP, since the results obtained for adsorbed DMMP are closer to those for the real nerve agent GA **[19]**.

A computational study **[134,135]** on the molecular and dissociative adsorption of DMMP on rutile and anatase forms of TiO_2, as well as on clusters with unsaturated edge atoms terminated with pseudohydrogen, enabled a comparative study of adsorption on periodic and non-periodic structures. For molecular adsorption, dative bond formation between $Ti_{5c}\cdots O{=}P$ at the unsaturated, 5-fold coordinated Ti surface site was reported. While interaction of the DMMP methyl group with the surface oxygen via a C-H···O bond contributed to stabilizing the target molecule, little or no contribution was obtained for the methoxy O atom interaction with Ti_{5c}. Of the several hypothetically possible products considered for dissociative adsorption, a $(CH_3)(CH_3O)P(\text{-}O\text{-})_2$ bridge between two Ti_{5c} sites, together with a CH_3 bonded to the O atom of a $(Ti\text{-})_2O_{2c}$ site, was considered most favorable. The adsorption energies for the cluster models were found to be consistent with those of the periodic models, though ΔE_{ads} is slightly higher for the cluster calculations **[134]**. Also, as expected, dissociative adsorption is more exothermic than molecular adsorption. Extension of this study **[136]** to the adsorption of DMMP on the TiO_2 anatase (001) surface, showed that adsorption in this case also occurs via Ti—O=P dative bond formation to a coordinatively unsaturated surface Ti site. One of the two Ti-O-Ti bridge bonds at the Ti adsorption site breaks, leading to the formation of a stable Ti=O titanyl group, a species that had never been reported in previous studies of adsorption on TiO_2 surfaces.

Another molecular and dissociative adsorption study of DMMP **[137]** used the cluster quantum-chemical method to elucidate the possible mechanism of destructive adsorption of DMMP on MgO nanoparticles. In consonance with the results for TiO_2 **[134]**, dissociative adsorption of DMMP was found to be thermodynamically favored over molecular adsorption to a single Lewis acid Mg^{2+} site on a 24 atom, two-layer model of the MgO (001) plane. The authors also considered a molecular adsorption pathway involving two Mg^{2+} sites, which was found to be unfavorable. According to the hypothesis proposed by the authors for decomposition of DMMP, a surface bound complex is formed as a result of molecular adsorption, and then dissociative adsorption takes place on increasing the temperature. The adsorption is followed by elimination of a

methoxy group from DMMP, which is subsequently adsorbed on a neighboring hydroxylated site. This methoxy group could be further oxidized by the phosphoryl oxygen of another DMMP molecule to produce formic acid and $(CH_3O)_2PCH_3$, or could react with water to form methanol. Calculations also inferred that ions with reduced coordination are thermodynamically more favorable sites for molecular and dissociative adsorption of DMMP. This again proves the fact that edge and corner sites possess greater reactivity and hence serve as better adsorbents.

DMMP and real agent's comparison study

Studies offering a comprehensive approach for comparison of DMMP with its real nerve agents were carried out by various research groups **[138-141]**. Bermudez **[138]** studied the adsorption of DMMP and the corresponding real agent GB on γ-Al_2O_3, using two different clusters, Al_8O_{12} and $Al_{20}O_{30}$, generated from bulk γ-Al_2O_3. Out of the three modes investigated in their work, the energetically favored mode of adsorption was found to be Al-O=P dative-bond formation, in close correspondence with deductions from the experimentally obtained infrared spectra. In contrast to previous studies **[17]**, the adsorption energy for DMMP was found to be about 8% smaller for Al_8O_{12} than for the $Al_{20}O_{30}$ cluster, signifying weaker interactions in the smaller cluster. A difference of about 12% in adsorption energy was found between the B3LYP/6-31G* and B3LYP/6-311G(df) levels, with lower energy for the former. The adsorption energies on the $Al_{20}O_{30}$ cluster for DMMP and GB were found to be comparable (ΔE_{ads} = -57.5 kcal mol^{-1} for DMMP and -49.2 kcal mol^{-1} for GB), signifying that DMMP is a good simulant for GB.

Bermudez **[140]** then analyzed the effects of surface hydroxylation and photolysis for the adsorption of DMMP, GB and VX on the surface of γ-Al_2O_3. The binding mode for the three molecules on the unhydroxylated Al_2O_3 surface was found to be the same as observed before **[138]**, i.e. for all three species, adsorption occurs via the Al(T_d)-O=P dative bond to an unsaturated tetrahedral Al(T_d) site. In case of VX, Al···N or Al···S dative bonding is not very favorable.

Hydroxylation

Studies on adsorption on the hydroxylated surface showed that, although OH···O=P bonding is the expected mode of adsorption for the hydroxylated surface, dative bonding remains the most stable mode when OH-free Al(T_d) sites are available. Even on a fully-OH covered surface, only a single OH···O=P bond is formed, demonstrating the less relevant role of the hydroxylated surface as adsorbent. Some contribution to adsorption is also made by weaker CH···O bonds involving alkyl groups. Again, for hydrogen-bond formation, the phosphoryl O atom of DMMP, VX and GB is favored over other active centers like the alkoxy O atom. The presence of the tertiary amine group makes VX basic enough to extract a proton from an acidic OH site, but due to its larger size, steric hindrance strongly affects its adsorption on the larger cluster. However, GB and DMMP (for which steric effects appear to be less important) display similar adsorption characteristic on both clusters.

Photolysis

Bermudez **[140]** studied the photochemical excitation of CWA when adsorbed on a photochemically inert oxide, in order to see if photochemistry can be induced in DMMP, GB and VX by sunlight. The results indicated that DMMP and GB could not serve the purpose, since the threshold for their electronic excitation, both in gas phase or when adsorbed on γ-Al_2O_3, lie in the vacuum ultraviolet (~7.1 eV or higher), which is much beyond the upper limit of the terrestrial solar spectrum (~4.5 eV). However, the photochemistry exhibited by VX was found to be interesting. In the gas phase, the threshold is ~4.2 eV, which shifts to a lower value of around 3.9 eV on the OH-free surface, where VX adsorbs via an Al(T_d)···O=P dative bond. On the other hand, VX bound to the hydroxylated surface via an OH···O=P dative bond shows a shift in adsorption to a higher value of about 4.3 eV. The change in excitation threshold for all the three species is attributed to shifts in molecular orbitals. It is clear from the results that for VX, photochemistry can be induced by sunlight since all excitation thresholds lie in the range of the terrestrial solar spectrum. Another interesting result which can be inferred is that even the photolytic properties of DMMP and GB are in accord with each other.

The mechanism of DMMP adsorption on the SiO_2 surface differs from that on other metal oxides, as revealed by experiments. Therefore, Bermudez **[139]** carried out *ab initio* quantum chemical calculations to study the interaction of TCP (trichloro phosphate), DMMP and GB on the amorphous SiO_2 surface. Adsorption on two SiO_2 models was considered: a small $Si_5O_7H_8$ "cagelike" cluster and a larger $Si_{21}O_{56}H_{28}$ model, and it was found that the larger model gives better adsorption results. The author attributed this behavior to the rigidity of the $Si_5O_7H_8$ structure, which consists of fused siloxane rings with only three or four Si atoms, as opposed to the "loose" and open structure of the large-cluster model. For all the three species studied, hydrogen bond formation between the O atom of the P=O group and the two Si-OH groups is the most energetically favorable adsorption mechanism, which is in accord with experimental results (infrared spectroscopy data). Any possibility of hydrogen bonding to the alkoxy atom of DMMP and GB and to the F atom of GB was found to be less favorable. The characteristics of DMMP and GB adsorption on the amorphous SiO_2 surface are closely similar, in the sense that no covalent bond is formed and weak interaction is reported. The fact that the computed adsorption energies of the two species are almost alike suggests that DMMP is a good simulant for GB in this regard also.

DMMP adsorption behavior was compared with that of another agent of the G-series, GA **[141]** by modeling the ZnO surface as $(ZnO)_n$ (n = 4, 18) molecular clusters of non-polar and polar surfaces. The adsorption of DMMP and GA on both polar and non-polar surfaces proceeds as chemisorption, but the latter is energetically more favorable. The larger positive charge on Zn increases its bonding ability with the target molecule. The results display only one mode of possible interaction in case of DMMP, that is, Zn···O bond formation, whereas GA adsorption can occur both through covalent bond formation between the molecular P atom and the surface O atom (in the case of the

small GA-Zn_4O_4 complex) or between the N atom of GA and the Zn atom of the surface (large GA-$Zn_{18}O_{18}$ system). A point to be noted is that, although the adsorption modes for DMMP and GA molecules on the ZnO surface are different, the binding energies for both are almost the same, with somewhat more negative values for GA.

Conclusion

The threat of terrorist attacks has spurred experimental and theoretical research on CWA. Metal oxides, because of their ready availability, have been the subjects of such studies, and many different metal oxides have been investigated in this regard. Nanoscale metal oxides are more reactive because of the presence of low-coordination and defect sites, corners, edges, hydroxylated sites, etc. The products of degradation of CWA on metal oxide nanosurfaces have been examined experimentally. For example, the products on the alumina surface are salts, which erode the surface, exposing new alumina surface for adsorption, making the decontamination even more effective. The finding that the products of degradation are usually benign is very encouraging. The use of sunlight for photochemical degradation on TiO_2 surfaces has also been explored, but complete degradation of the CWA only takes place on 6 h of exposure. The correlation found between the results for the G-agents and their simulant DMMP implies that experiments performed with the simulant can be extrapolated to understand the mechanism for the real agents. Though a lot of data regarding the adsorption and degradation of CWA on nanoscale metal oxides has accumulated over the years, a lot more experimental and theoretical work needs to be done to find materials for the early detection and decontamination of CWA. In particular, mixed metal oxide nanoparticles need to be explored further, as they have shown promise as future materials for CWA adsorption and degradation.

Acknowledgements

NS thanks the Council for Scientific and Industrial Research (CSIR), New Delhi, for a Senior Research Fellowship and for financial support (Grant No. 01(2554)/12/EMR-1).

Reference

1. Marrs, T. C.; Maynard, R. L.; Sidell, F. R. *Chemical Warfare Agents: Toxicology and Treatment*, John Wiley and Sons: Chichester, **1996**, pp. 145.
2. Munro, N. B.; Ambrose, K. R.; Watson, A. P. *Environ. Health Perspect.* **1994**, *102*, 18.
3. Vijayaraghavan, R.; Kulkarni, A.; Pant, S. C.; Kumar, P.; Rao, P. V. L.; Gupta, N.; Gautam, A.; Ganesan, K. *Toxicol. Appl. Pharmacol.* **2005**, *202*, 180. **DOI:** 10.1016/j.taap.2004.06.020
4. Watson, A. P.; Opresko, D. M.; Young, R. A.; Hauschild, V. *J. Toxicol. Environ. Health B* **2006**, *9*, 173. **DOI:** 10.1080/15287390500194441
5. Corbridge, D. *Phosphorus: An Outline of its Chemistry, Biochemistry and Technology* Elsevier: Amsterdam, **1976**, pp. 319.
6. Emsley, J.; Hall, D. *The Chemistry of Phosphorus* Harper & Row: New York, **1976**, pp. 502-508.
7. Heath, D. F. *Organophosphorus Poisons* Pergamon Press: London, **1961**.
8. Miao. Z.; Du. Z. *Bopuxue Zazhi* **1989**, *6*, 469.
9. van den Berg; G. R.; Beck, H. C.; Benschop, H. P. *Bull. Environ. Contam. Toxicol.* **1984**, *33*, 505. **DOI:** 10.1007/BF01625576
10. Benshop, H. P.; de Jong, L. P. A. *Acc. Chem. Res.* **1988**, *21*, 368. **DOI:** 10.1021/ar00154a003
11. Koehler, K. F.; Zaddach, H.; Kuntsevich, A. D.; Chervin, I. I.; Kostyanovsky, R. G. *Russ. Chem. Bull.* **1993**, *42*, 1611. **DOI:** 10.1007/BF00699210
12. Degenhardt, C. E. A. M.; van den Berg, G. R.; De Jong, L. P. A.; Benschop, H. P.; van Genderen, J.; van de Meent, D. *J. Am. Chem. Soc.* **1986**, *108*, 8290. **DOI:** 10.1021/ja00286a043
13. Ekström, F.; Akfur, C.; Tunemalm, A. -K.; Lundberg, S. *Biochemistry* **2006**, *45*, 74. **DOI:** 10.1021/bi051286t
14. Ekerdt, J. G.; Klabunde, K. J.; Shapley, J. R.; White, J. M.; Yates, J. T. Jr. *J. Phys. Chem.* **1988**, *92*, 6182. **DOI:** 10.1021/j100333a005
15. Mawhinney, D. B.; Rossin, J. A.; Gehart, K.; Yates, J. T. Jr. *Langmuir* **1999**, *15*, 4789. **DOI:** 10.1021/la981440v
16. Wagner, G. W.; Bartram, P. W. Interaction of VX, G and HD simulants with self decontaminating sorbents. A solid state NMR study. ERDEC-TR-375, Aberdeen Proving Ground, MD, **1996**.
17. Michalkova, A.; Ilchenko, M.; Gorb, L.; Leszczynski, J. *J. Phys. Chem. B* **2004**, *108*, 5294. **DOI:** 10.1021/jp036766d
18. Wagner, G. W.; Bartram, P. W.; Koper, O.; Klabunde, K. J. *J. Phys. Chem. B* **1999**, *103*, 3225. **DOI:** 10.1021/jp984689u
19. Michalkova, A.; Paukku, Y.; Majumdar, D.; Leszczynski, *J. Chem. Phys. Lett.* **2007**, *438*, 72. **DOI:** 10.1016/j.cplett.2007.02.066
20. Wagner, G. W.; Koper, O. B.; Lucas, E.; Decker, S.; Klabunde, K. J. *J. Phys. Chem. B* **2000**, *104*, 5118. **DOI:** 10.1021/jp000101j
21. Kuiper, A. E. T.; van Bokhoven, J. J. G. M.; Medema, J. *J. Catal.* **1976**, *43*, 154. **DOI:** 10.1016/0021-9517(76)90302-X
22. Saxena, A.; Singh, B.; Srivastava, A. K.; Suryanarayana, M. V. S.; Ganesan, K.; Vijayaraghavan, R.; Dwivedi, K. K. *Microporous Mesoporous Mater.* **2008**, *115*, 364. **DOI:** 10.1016/j.micromeso.2008.02.007
23. Saxena, A.; Sharma, A.; Srivastava, A. K.; Singh, B.; Gutch, P. K.; Semwal, R. P. *J. Chem. Technol. Biotechnol.* **2009**, *84*, 1860. **DOI:** 10.1002/jctb.2258
24. Saxena, A.; Srivastava, A. K.; Singh, B.; Gupta, A. K.; Suryanarayana, M. V. S.; Pandey, P. *J. Hazard. Mater.* **2010**, *175*, 795. **DOI:** 10.1016/j.jhazmat.2009.10.078
25. Wagner, G. W.; Procell, L. R.; O'Connor, R. J.; Munavalli, S.; Carnes, C. L.; Kapoor, P. N.; Klabunde, K. J. *J. Am. Chem. Soc.* **2001**, *123*, 1636. **DOI:** 10.1021/ja003518b
26. Hirakawa, T.; Sato, K.; Komano, A.; Kishi, S.; Nishimoto, C. K.; Mera, N.; Kugishima, M.; Sano, T.; Ichinose, H.; Negishi, N.; Seto, Y.; Takeuchi, K. *J. Phys. Chem. C* **2010**, *114*, 2305. **DOI:** 10.1021/jp910911x
27. Naseri, M. T.; Sarabadani, M.; Ashrafi, D.; Saeidian, H.; Babri, M. *Environ. Sci. Pollut. Res.* **2012**. **DOI:** 10.1007/s11356-012-0997-7
28. Prasad, G. K.; Mahato, T. H.; Singh, B.; Ganesan, K.; Srivastava, A. R.; Kaushik, M. P.; Vijayaraghavan, R. *AIChE J.* **2008**, *54*, 2957. **DOI:** 10.1002/aic.11598
29. Prasad, G. K.; Singh, B.; Ganesan, K.; Batra, A.; Kumeria, T.; Gutch, P. K.; Vijayaraghavan, R. *J. Hazard. Mater.* **2009**, *167*, 1192. **DOI:** 10.1016/j.jhazmat.2009.01.129
30. Ramacharyulu, P. V. R. K.; Prasad, G. K.; Ganesan, K.; Singh, B. *J. Mol. Catal. A: Chem.* **2012**, *353-354*, 132. **DOI:** 10.1016/j.molcata.2011.11.016
31. Sato, K.; Hirakawa, T.; Komano, A.; Kishi, S.; Nishimoto, C. K.; Mera, N.; Kugishima, M.; Sano, T.; Ichinose, H.; Negishi, N.; Seto, Y.; Takeuchi, K. *Appl. Catal. B: Environ.* **2011**, *106*, 316. **DOI:** 10.1016/j.apcatb.2011.05.032
32. Štengl, V.; Maříková , M.; Bakardjieva, S.; Šubrt, J.; Opluštil F.; Olšanská, M. *J. Chem. Technol. Biotechnol.* **2005**, *80*, 754. **DOI:** 10.1002/jctb.1218
33. Štengl, V.; Grygara, T. M.; Opluštil, F.; Němec, T. *J. Hazard. Mater.* **2012**, *227-228*, 62. **DOI:** 10.1016/j.jhazmat.2012.05.007

34. Wagner, G. W.; Chen, Q.; Wu, Y. *J. Phys. Chem. C* **2008**, *112*, 11901. **DOI:** 10.1021/jp803003k
35. Wagner, G. W.; Peterson, G. W.; Mahle, J. J. *Ind. Eng. Chem. Res.* **2012**, *51*, 3598. **DOI:** 10.1021/ie202063p
36. Mahato, T. H.; Prasad, G. K.; Singh, B.; Acharya, J.; Srivastava, A. R.; Vijayaraghavan, R. *J. Hazard. Mater.* **2009**, *165*, 928. **DOI:** 10.1016/j.jhazmat.2008.10.126
37. Prasad, G. K.; Mahato, T. H.; Singh, B.; Ganesan, K.; Pandey, P.; Sekhar, K. *J. Hazard. Mater.* **2007**, *149*, 460. **DOI:** 10.1016/j.jhazmat.2007.04.010
38. Prasad, G. K.; Ramacharyulu, P. V. R. K.; Singh, B.; Batra, K.; Srivastava, A. R.; Ganesan, K.; Vijayaraghavan, R. *J. Mol. Catal. A: Chem.* **2011**, *349*, 55. **DOI:** 10.1016/j.molcata.2011.08.018
39. Kakkar, R.; Kapoor, P. N.; Klabunde, K. J. *J. Phys. Chem. B* **2004**, *108*, 18140. **DOI:** 10.1021/jp0470546
40. Kakkar, R.; Kapoor, P. N.; Klabunde, K. J. *J. Phys. Chem. B* **2006**, *110***,** 25941. **DOI:** 10.1021/jp0603536
41. Yang, Y. -C.; Baker, J. A.; Ward, J. R. *Chem. Rev.* **1992**, *92*, 1729. **DOI:** 10.1021/cr00016a003
42. Yang, Y. -C. *Acc. Chem. Res.* **1999**, *32*, 109.
43. Yang, Y. -C.; Szafraniec, L. L.; Beaudry, W. T.; Bunton, C. A. *J. Org. Chem.* **1993**, *58*, 6964. **DOI:** 10.1021/jo00077a011
44. Wagner, G. W.; Bartram, P. W. *J. Mol. Catal. A. Chem.* **1996**, *111*, 175. **DOI:** 10.1016/1381-1169(96)00226-9
45. Wagner, G. W.; Bartram, P. W. *J. Mol. Catal. A. Chem.* **1999**, *144*, 419. **DOI:** 10.1016/S1381-1169(98)00343-4
46. Jang, B. W. -L.; Spivey, J. J. *Catal. Today* **2000**, *55*, 3. **DOI:** 10.1016/S0920-5861(99)00221-7
47. Driessen, M. D.; Miller, T. M.; Grassian, V. H. *J. Mol. Catal. A: Chem.* **1998**, *131*, 149. **DOI:** 10.1016/S1381-1169(97)00262-8
48. Sehili, T.; Boule, P.; Lemaire, J. *J. Photochem. Photobiol. A* **1989**, *50*, 103. **DOI:** 10.1016/1010-6030(89)80024-3
49. Villaseñor, J.; Reyes, P.; Pecchi, G. J. *Chem. Technol. Biotechnol.* **1998**, *72*, 105. **DOI:** 10.1002/(SICI)1097-4660(199806)72:2<105::AID-JCTB883>3.0.CO;2-0
50. Yun, K. -H.; Yun, K. -Y.; Cha, G. -Y.; Lee, B. -H.; Kim, J. -C.; Lee, D. -D.; Huh, J. -S. *Mater. Sci. Forum* **2005**, *486-487*, 9. **DOI:** 10.4028/www.scientific.net/MSF.486-487.9
51. Richard, C.; Bosquet, F.; Pilichowski, J. -F. *J. Photochem. Photobiol. A: Chem.* **1997**, *108*, 45. **DOI:** 10.1016/S1010-6030(96)04431-0
52. Yeber, M. C.; Rodríguez, J.; Freer, J.; Duŕan, N.; Mansilla, H. D. *Chemosphere* **2000**, *41*, 1193. **DOI:** 10.1016/S0045-6535(99)00551-2
53. Lin, Y.; Zhang, Z.; Tang, Z.; Yuan, F.; Li, J. *Adv. Mater. Opt. Electron.* **1999**, *9*, 205. **DOI:** 10.1002/1099-0712(199909/10)9:5<205::AID-AMO383>3.0.CO;2-8
54. Aurian-Blajeni, B.; Boucher, M. M. *Langmuir* **1989**, *5*, 170.**DOI:** 10.1021/la00085a032
55. Yang, Y. -C.; Szafraniec, L. L.; Beaudry W. T.; Ward, J. R. *J. Org. Chem.* **1988**, *53*, 3293. **DOI:** 10.1021/jo00249a029
56. Mahato, T. H.; Prasad, G. K.; Singh, B.; Srivastava, A. R.; Ganesan, K.; Acharya, J.; Vijayaraghavan, R. *J. Hazard. Mater.* **2009**, *166*, 1545. **DOI:** 10.1016/j.jhazmat.2008.11.073
57. Bailey, S. W. *Structures of Layered Silicates.* In *Crystal Structures of Clay Minerals and their X-ray Identification* Brindley, G. W. & Brown, G. (Eds.) Mineralogical Society: London, **1980**, pp. 6-28.
58. Raussell-Colom, J. A.; Serratosa, J. M. *The Chemistry of Clays and Clay Minerals* Newman, A. C. D. (Ed.) Mineralogical Society Monograph No. 6; Longman Scientific & Technical: London, **1987**, Ch-8, pp. 480.
59. Bates, R. L. *Stone, Clay, Glasses: How Building Materials are Found and Used*. Erslow: New York, **1987**.
60. Grim, R. E. *Clay mineralogy* McGraw-Hill Book Company, Inc., New York, **1953**.
61. Michalkova, A.; Gorb, L.; Ilchenko, M.; Zhikol, O. A.; Shishkin, O. V.; Leszczynski, J. *J. Phys. Chem. B* **2004**, *108*, 1918. **DOI:** 10.1021/jp030391e
62. Michalkova, A.; Martinez, J.; Zhikol, O. A.; Gorb, L.; Shishkin, O. V.; Leszczynska, D.; Leszczynski, J. *J. Phys. Chem. B* **2006**, *110*, 21175. **DOI:** 10.1021/jp062306j
63. Murashov, V. V.; Leszczynski, J. *J. Phys. Chem. A* **1999**, *103*, 1228. **DOI:** 10.1021/jp981996r
64. Hartzell, C. J.; Cygan, R. T.; Nagy, K. L. *J. Phys. Chem. A* **1998**, *102*, 6722. **DOI:** 10.1021/jp981089m
65. Turpault, M. -P.; Trotignon, L. G*eochim. Cosmochim. Acta* **1994**, *58*, 2761. **DOI:** 10.1016/0016-7037(94)90112-0
66. Charlet, L.; Schindler, P. W.; Spadini, L.; Furrer, G.; Zysset, M. *Aquat. Sci.* **1993**, *55*, 291. **DOI:** 10.1007/BF00877274
67. Schlegel, M. L.; Manceau, A.; Chateigner, D.; Charlet, L. *J. Colloid Interface Sci.* **1999**, *215*, 140. **DOI:** 10.1006/jcis.1999.6253
68. White G. N.; Zelazny, L. W. *Clays Clay Miner.* **1988**, *36*, 141.
69. Zachara, J. M.; McKinley, J. P. *Aquat. Sci.* **1993**, *55*, 250. **DOI:** 10.1007/BF00877270
70. Gautam, A.; Vijayaraghavan, R.; Sharma, M.; Ganesan, K. *J. Med. CBR Def.* **2006**, *4*, 1.
71. Rowland, J. C.; Brower, M. E.; Roberts, W. C. Health advisory for dimethyl methylphosphonate. Environmental Protection Agency, Washington, DC, **1992**.
72. Bingham, E.; Cohrssen, B.; Powell, C. H. *Patty's Toxicology* Volumes 1-9 5th ed. John Wiley & Sons. New York, **2001**, pp. 6: 950t.
73. Lewis, R. J. *Sax's Dangerous Properties of Industrial Materials.* Van Nostrand Reinhold, New York, **1996**.
74. EA, Japan Investigation of the ecotoxicological effects of OECD high production volume chemicals. Office of Health Studies, Environmental Health Department, Environment Agency, Japan (HPV/SIDS Test conducted by EA, Japan), **1994**.
75. Agricultural Research Service, USDA Information Memorandum, **1966** Vol. 20, pp. 7.
76. Izmerov, N. F.; Sanotsky, I. V.; Sidorov, K. K. Toxicometric parameters of industrial toxic chemicals under single exposure. Moscow, Russia: Centre of International Projects, GKNT, **1982**, pp. 56.
77. Tomlin, C. The Pesticide Manual: A World Compendium (10th ed.), British Crop Protection Council, Surrey, United Kingdom, **1994**.
78. Yue, Z.; Mangun, C.; Economy, J.; Kemme, P.; Cropek, D.; Maloney, S. *Environ. Sci. Technol.* **2001**, *35*, 2844. **DOI:** 10.1021/es001858r
79. Groenewold, G. S.; Ingram, J. C.; Appelhans, A. D.; Delmore, J. E.; Dahl, D. A. *Environ. Sci. Technol.* **1995**, *29*, 2107. **DOI:** 10.1021/es00008a033
80. Wagner, G. W.; MacIver, B. K. *Langmuir* **1998**, *14*, 6930. **DOI:** 10.1021/la9805037
81. Wagner, G. W.; Bartram, P. W. *Langmuir* **1999**, *15*, 8113. **DOI:** 10.1021/la990716b
82. Raber, E.; McGuire, R. *J. Haz. Mater.* **2002**, *93*, 339. **DOI:** 10.1016/S0304-3894(02)00051-1
83. Singer, B. C.; Hodgson, A. T.; Destaillats, H.; Hotchi, T.; Revzan, K. L.; Sextro, R. G. *Environ. Sci. Technol.* **2005**, *39*, 3203. **DOI:** 10.1021/es049144u
84. Mangun, C. L.; Yue, Z.; Economy, J.; Maloney, S.; Kemme, P.; Cropek, D. *Chem. Mater.* **2001**, *13*, 2356. **DOI:** 10.1021/cm000880g
85. Gordon, W. O.; Tissue, B. M.; Morris, J. R. *J. Phys. Chem. C* **2007**, *111*, 3233. **DOI:** 10.1021/jp0650376
86. Paukku, Y.; Michalkova, A.; Leszczynski, J. *Struct. Chem.* **2008**, *19*, 307. **DOI:** 10.1007/s11224-008-9287-x
87. Waghe, A.; Kanan, S. M.; Abu-Yousef, I.; Jensen, B.; Tripp, C. P. *Res. Chem. Intermediat.* **2006**, *32*, 613. **DOI:** 10.1163/156856706778400280

88. Borrett, V. T.; Gan, T. –H.; Lakeland, B. R.; Leslie, D. R.; Mathews, R. J.; Mattsson, E. R.; Riddell, S.; Tantaro, V. *J. Chromatogr. A* **2003**, *1003*, 143. **DOI:** 10.1016/S0021-9673(03)00774-X
89. Bennett, S. R.; Bane, J. M.; Benford, P. J.; Pyatt, R. L. Environmental hazards of chemical agent simulants, CRDC-TR-84055, U. S. Army Chemical Research and Development Center, Aberdeen Proving Ground, MD, **1984**.
90. Hoskin, F. C. G.; Walker, J. E. *Bull. Environ. Contam. Toxicol.* **1997**, 59, 9. **DOI:** 10.1007/s001289900436
91. Seabolt, E. E.; Ford, W. T. *Langmuir* **2003**, *19*, 5378. **DOI:** 10.1021/la030051k
92. Bertilsson, L.; Potje-Kamloth, K.; Liess, H. -D.; Engquist, I.; Liedberg, B. *J. Phys. Chem. B.* **1998**, *102*, 1260. **DOI:** 10.1021/jp973215c
93. Kanan, S. M.; Lu, Z.; Tripp, C. P. *J. Phys. Chem. B* **2002**, *106*, 9576. **DOI:** 10.1021/jp014647x
94. Kim, C. S.; Lad, R. J.; Tripp, C. P. *Sens. Actuators B* **2001**, *76*, 442. **DOI:** 10.1016/S0925-4005(01)00653-0
95. Hegde, R. I.; White, J. M. *Appl. Surf. Sci.* **1987**, *28*, 1. **DOI:** 10.1016/0169-4332(87)90024-9
96. Henderson, M. A.; Jin, T.; White J. M. *J. Phys. Chem.* **1986**, *90*, 4607. **DOI:** 10.1021/j100410a027
97. Mitchell, M. B.; Sheinker, V. N.; Mintz, E. A. *J. Phys. Chem. B* **1997**, *101*, 11192. **DOI:** 10.1021/jp972724b
98. Segal, S. R.; Cao, L.; Suib, S. L.; Tang, X.; Satyapal, S. *J. Catal.* **2001**, *198*, 66. **DOI:** 10.1006/jcat.2000.3126
99. Kozlova, E. A.; Vorontsov, A. V. *Appl. Catal. B* **2006**, *63*, 114. **DOI:** 10.1016/j.apcatb.2005.09.020
100. Mera, N.; Hirakawa, T.; Sano, T.; Takeuchi, K.; Seto, Y.; Negishi, N. *J. Hazard. Mater.* **2010**, *177*, 274. **DOI:** 10.1016/j.jhazmat.2009.12.029
101. Moss, J. A.; Szczepankiewicz, S. H.; Park, E.; Hoffmann, M. R. *J. Phys. Chem. B* **2005**, *109*, 19779. **DOI:** 10.1021/jp052057j
102. Rusu, C. N.; Yates, J. T. Jr. *J. Phys. Chem. B* **2000**, *104*, 12299. **DOI:** 10.1021/jp002562a
103. Rusu, C. N.; Yates, J. T. Jr. *J. Phys. Chem. B* **2000**, *104*, 12292. **DOI:** 10.1021/jp002560q
104. Trubitsyn, D. A.; Vorontsov, A. V. *J. Phys. Chem. B* **2005**, *109*, 21884. **DOI:** 10.1021/jp053793q
105. Zhou, J.; Varazo, K.; Reddic, J. E.; Myrick, M. L.; Chen, D. A. *Anal. Chim. Acta* **2003**, *496*, 289. **DOI:** 10.1016/S0003-2670(03)01008-0
106. Bermudez, V. M. *Langmuir* **2010**, *26*, 18144. **DOI:** 10.1021/la103381r
107. Sheinker, V. N.; Mitchell, M. B. *Chem. Mater.* **2002**, *14*, 1257. **DOI:** 10.1021/cm010758x
108. Templeton, M. K.; Weinberg, W. H. *J. Am. Chem. Soc.* **1985**, *107*, 774. **DOI:** 10.1021/ja00290a006
109. Templeton, M. K.; Weinberg, W. H. *J. Am. Chem. Soc.* **1985**, *107*, 97. **DOI:** 10.1021/ja00287a018
110. Kanan, S. M.; Tripp, C. P. *Langmuir* **2001**, *17*, 2213. **DOI:** 10.1021/la001624l
111. Kanan, S. M.; Tripp, C. P. *Langmuir* **2002**, *18*, 722. **DOI:** 10.1021/la011253o
112. Quenneville, J.; Taylor, R. S.; van Duin, A. C. T. *J. Phys. Chem. C* **2010**, *114*, 18894. **DOI:** 10.1021/jp104547u
113. Saxena, A.; Srivastava, A. K.; Singh, B.; Goyal, A. *J. Hazard. Mater.* **2012**, *211-212*, 226. **DOI:** 10.1016/j.jhazmat.2011.07.117
114. Wilmsmeyer, A. R.; Uzarski, J.; Barrie, P. J.; Morris, J. R. *Langmuir* **2012**, *28*, 10962. **DOI:** 10.1021/la301938f
115. Li, Y. -X.; Schlup, J. R.; Klabunde, K. J. *Langmuir* **1991**, *7*, 1394. **DOI:** 10.1021/la00055a018
116. Lin, S. -T.; Klabunde, K. J. *Langmuir* **1985**, *1*, 600. **DOI:** 10.1021/la00065a015
117. Cao, L.; Segal, S. R.; Suib, S. L.; Tang, X.; Satyapal, S. *J. Catal.* **2000**, *194*, 61. **DOI:** 10.1006/jcat.2000.2914
118. Mitchell, M. B.; Sheinker, V. N.; Cox, W. W. Jr.; Gatimu, E. N.; Tesfamichael, A. B. *J. Phys. Chem. B* **2004**, *108*, 1634. **DOI:** 10.1021/jp035590c
119. Tesfai, T. M.; Sheinker, V. N.; Mitchell, M. B. *J. Phys. Chem. B* **1998**, *102*, 7299. **DOI:** 10.1021/jp980690h
120. Ma, S.; Zhou, J.; Kang, Y. C.; Reddic, J. E.; Chen, D. A. *Langmuir* **2004**, *20*, 9686. **DOI:** 10.1021/la048594x
121. Zhou, J.; Ma, S.; Kang, Y. C.; Chen, D. A. *J. Phys. Chem. B* **2004**, *108*, 11633. **DOI:** 10.1021/jp040185m
122. Li, Y. -X.; Klabunde, K. J. *Langmuir* **1991**, *7*, 1388. **DOI:** 10.1021/la00055a017
123. Li, Y. -X.; Koper, O.; Atteya, M.; Klabunde, K. J. *Chem. Mater.* **1992**, *4*, 323. **DOI:** 10.1021/cm00020a019
124. Decker, S. P.; Klabunde, J. S.; Khaleel, A.; Klabunde, K. J. *Environ. Sci. Technol.* **2002**, *36*, 762. **DOI:** 10.1021/es010733z
125. Jiang, Y.; Decker, S.; Mohs, C.; Klabunde, K. J. *J. Catal.* **1998**, *180*, 24. **DOI:** 10.1006/jcat.1998.2257
126. Nazari, B.; Jaafari, M. *Dig. J. Nanomater. Bios.* **2010**, *5*, 909.
127. Mattsson, A.; Lejon, C; Štengl, V.; Bakardjieva, S.; Opluštil, F.; Andersson , P. O.; Österlund, L. *Appl. Catal. B: Environ.* **2009**, *92*, 401. **DOI:** 10.1016/j.apcatb.2009.08.020
128. Panayotov, D. A.; Morris, J. R. *J. Phys. Chem. C* **2009**, *113*, 15684. **DOI:** 10.1021/jp9036233
129. Panayotov, D. A.; Morris, J. R. *Langmuir* **2009**, *25*, 3652. **DOI:** 10.1021/la804018b
130. Patil, L. A.; Bari, A. R.; Shinde, M. D.; Deo, V.; Kaushik, M.P. *Sens. Actuators B* **2012**, *161*, 372. **DOI:** 10.1016/j.snb.2011.10.047
131. Chen, D. A.; Ratliff, J. S.; Hua, X.; Gordon, W. O.; Senanayake, S. D.; Mullins, D. R. *Surf. Sci.* **2010**, *604*, 574. **DOI:** 10.1016/j.susc.2009.12.028
132. Mitchell, M. B.; Sheinker, V. N.; Tesfamichael, A. B.; Gatimu, E. N.; Nunley, M. *J. Phys. Chem. B* **2003**, *107*, 580. **DOI:** 10.1021/jp021836m
133. Obee, T. N.; Satyapal, S. *J. Photochem. Photobiol. A: Chem.* **1998**, *118*, 45. **DOI:** 10.1016/S1010-6030(98)00372-4
134. Bermudez, V. M. *J. Phys. Chem. C* **2010**, *114*, 3063. **DOI:** 10.1021/jp9098304
135. Bermudez, V. M. *Surf. Sci.* **2010**, *604*, 706. **DOI:** 10.1016/j.susc.2010.01.021
136. Bermudez, V. M. *J. Phys. Chem. C* **2011**, *115*, 6741. **DOI:** 10.1021/jp200009s
137. Zhanpeisov, N. U.; Zhidomirov, G. M.; Yudanov, I. V.; Klabunde, K. J. *J. Phys. Chem.* **1994**, *98*, 10032. **DOI:** 10.1021/j100091a015
138. Bermudez, V. M. *J. Phys. Chem. C* **2007**, *111*, 3719. **DOI:** 10.1021/jp066439g
139. Bermudez, V. M. *J. Phys. Chem. C* **2007**, *111*, 9314. **DOI:** 10.1021/jp071529m
140. Bermudez, V. M. *J. Phys. Chem. C* **2009**, *113*, 1917. **DOI:** 10.1021/jp809053u
141. Paukku, Y.; Michalkova, A.; Leszczynski, J. *J. Phys. Chem. C* **2009**, *113*, 1474. **DOI:** 10.1021/jp807744a